Journal of Colloid and Interface Science, Volume 613, May 2022, pp. 376-383
DOI:10.1016/j.jcis.2022.01.046

AuAg nanocages/graphdiyne for rapid elimination and detection of trace pathogenic bacteria

Qiang Bai[a,1], Hongyang Luo[a,1], Shugao Shi[a], Shen Liu[a], Lina Wang [b, *], Fanglin Du[a], Zhugen Yang[c], Zhiling Zhu[a, *], Ning Sui[a, *]

[a] College of Materials Science and Engineering, Qingdao University of Science and Technology, 53 Zhengzhou Rd., Qingdao, Shandong 266042, China

[b] College of Environment and Safety Engineering, Qingdao University of Science and Technology, 53 Zhengzhou Rd., Qingdao, Shandong 266042, China

[c] Cranfield Water Science Institute, Cranfield University, Milton Keynes, MK43 0AL, UK

[1] Qiang Bai and Hongyang Luo contributed to this work equally

[*] Corresponding authors: L. Wang (lnwang2006@163.com); Z. Zhu (zlzhu@qust.edu.cn); N. Sui (suining@qust.edu.cn)

ABSTRACT

We prepared a biocompatible AuAg nanocages/graphdiyne@ polyethylene glycol (AuAg/GDY@PEG) composite. The combination of AuAg and GDY to obtain a synergistically enhanced photothermal effect, and the antibacterial effect of GDY and AuAg are used in combined anti-infective therapy. The in vitro antibacterial activity of AuAg/GDY@PEG was investigated, showing an impressive broad-spectrum antibacterial activity with the killing rate > 99.999%. Based on the photothermal conversion ability of AuAg/GDY@PEG, a simple photothermal immunoassay for pathogenic bacteria was successfully established. Sandwich immune response was performed on a microporous plate, the microplate containing the antibody binds specifically to the bacterium being tested, which then binds to the material with the antibody on its surface, and the signal was a change in temperature under 808 nm near-infrared light. The limit of detection (LOD) for *S. typhimurium* detection is 10^3 CFU·mL^{-1}, with a range of 10^3–10^7 CFU·mL^{-1}. This method is accurate, rapid and low-cost, which can be used for on-site detection of pathogenic bacteria in food.

KEYWORDS: Photothermal effect, Gold-silver nanocages, Graphdiyne, Immunoassay, Antibacterial

Published by Elsevier. This is the Author Accepted Manuscript issued with: Creative Commons Attribution Non-Commercial No Derivatives License (CC:BY:NC:ND 4.0).
The final published version (version of record) is available online at DOI:10.1016/j.jcis.2022.01.046. Please refer to any applicable publisher terms of use.

1. Introduction

Infectious diseases caused by either bacterial infections or microbial contamination food significantly threaten public health and have been considered as one of the greatest global issues [1, 2]. In recent years, a variety of antibiotics have been discovered and play a very important role in the treatment of bacterial infections. Due to the abuse of antibiotics, a large number of drug-resistant strains continue to emerge, causing significant threats on human health [3-5]. If the reproduction and transfer of bacteria can be detected at a low level, and they can be effectively eliminated in time, they can be effectively inhibited. As a result, researchers around the world are working to develop new antimicrobial method [6, 7] and detection method [8-10] to effectively combat drug-resistant bacterial infection.

Photothermal therapy (PTT) and photodynamic therapy (PDT) have become a promising anti-infection therapy because of the advantages of low toxicity, good selectivity and good repeatability [11]. The therapeutic effect of PDT is affected by oxygen content, and the short life span of reactive oxygen species also limits its effectiveness [12]. PTT has a deep therapeutic range due to the use of long wavelength and deep penetration range of near-infrared light, and photothermal agent does not need oxygen to play a role, so it may be an ideal anti-infection treatment method [13]. Photothermal effect has been widely studied and applied in antibacterial [14, 15] and cancer therapy [16, 17] because of the excellent photothermal conversion property of photothermal materials, involving in gold-based materials [11, 18], carbon-based materials [19, 20], and organic molecule dyes [21]. Recently, new applications of photothermal materials have been explored, in which photothermal biosensing emerged as a novel and attractive method in the quantitative detection of pathogenic bacteria and biomolecules [22, 23]. This method provides a simple, low-cost, and rapid, in which no

costly analytical instrument or specialized person is needed.

Near-infrared (NIR) laser inducing hyperthermia is generally the perfect choice due to the excellent tissue penetration capability. Graphdiyne (GDY) is a new carbon allotrope consisted of benzene rings and butadiyne linkages [24, 25], attractive structural and electronic properties make it a potential material for many applications [26], it is widely used in electrochemical energy [27-29], biomedicine [30], sensing [31] and catalysis [32, 33]. Studies have shown that GDY has a wide range of absorption from visible light to NIR light, and has a good photothermal conversion ability, and has a wide range of potential applications in photothermal therapy [30, 34, 35]. In addition, GDY is an excellent antimicrobial material [36-38]. The synergistic mechanism of bacterial membrane encapsulation, insertion, destruction and oxidative stress are may the source of the antimicrobial activity of GDY. The localized surface plasmon resonance (LSPR) of gold-silver nanocages (AuAg) can be adjusted in the NIR range by controlling the thickness of the gold shell [39]. The absorption of the gold cage in the near infrared region can be used to convert light into heat energy for photothermal treatment, have high efficiency of photothermal conversion. AuAg with hollow interior and porous walls have the advantage of easy surface functionalization and have been widely used in drug delivery [40], imaging [41], PTT [42] applications. AuAg have also been exploited as antimicrobial agents [11]. Silver nanoparticles are higher cytotoxic to microorganisms [43]. Therefore, silver-based compounds have been extensively studied in biomedical antibacterial research.

In this study, we combine AuAg, which has a NIR tunable LSPR peak, with GDY, which has extensive absorption from the visible to NIR range, enhanced photothermal performance is obtained. The LSPR peak of AuAg was shifted to about 800 nm to enhance the absorption of the material at 800 nm near infrared band. We investigated

the broad-spectrum antimicrobial activity of AuAg/GDY@PEG against *S. aureus* and *E. coli*, bacterial killing rate > 99.999%. The combination of AuAg and GDY to obtain a synergistically enhanced photothermal effect and the antibacterial effect of GDY are used in combined anti-infective therapy. A simple and convenient method was developed for the sensitive, rapid and accuracy detection of *S. typhimurium* based on the photothermal effect of AuAg/GDY@PEG，as shown in the Scheme.1. The excellent photothermal effect of AuAg/GDY@PEG was used to improve the detection sensitivity.

<Scheme 1>

2. Experimental

2.1 Synthesis of AuAg/GDY@PEG

The synthesis of GDY, Ag nanocubes and AuAg nanocages are shown in Supporting Information. The GDY (10 mg) was dispersed in 10 mL of water and mixed with 10 mg of polyethylene glycol (PEG, MW =6000) under sonication for 1 h. After sonication, excess PEG molecules were removed by centrifugation at 9000 rpm and washed with water for three times. The resulted AuAg/GDY@PEG was re-suspended in pure water to form GDY@PEG aqueous solution. The obtained AuAg and GDY@PEG solutions were added into the bottle according to the mass ratio of 1:1, stirred for 12 h and centrifuged (5000 rpm, 3 min) to remove the unloaded AuAg. The resulting precipitates were dispersed in distilled water.

2.2 Photothermal performance of AuAg/GDY@PEG

The photothermal properties of the materials were evaluated by heating curve and infrared thermal imaging. The AuAg/GDY@PEG, AuAg/GDY, AuAg+GDY(only physical mixing), AuAg and GDY solutions with equivalent concentration (AuAg or GDY) were irradiated under NIR (808 nm, 0.9 W cm^{-2}) for10 min. The water as the control group. Different concentrations (10, 20, 40, 80, 100 μg mL^{-1}) of AuAg/GDY@PEG were irradiated under NIR (808 nm, 0.9 W cm^{-2}) for 10 min. 80 μg

mL^{-1} of AuAg/GDY@PEG were irradiated under NIR (808 nm) with different powers (0.3, 0.4, 0.5, 0.7, and 0.9 W cm^{-2}) for 10 min. All above the temperature was recorded every 30 s, infrared thermal images were recorded by an infrared camera.

2.3 Bacterial cell culture

Staphylococcus aureus (ATCC 6538) and *Escherichia coli* (ATCC 25922) were purchased from the general microbiological culture collection center (CGMCC). The bacteria were cultured in LB medium overnight, in a shaker at 37 ° C at 200 rpm, then transferred to LB agar plates. In each experiment, a single colony of *S. aureus* or *E. coli* was taken from LB agar plate and cultured in LB medium at 200 rpm at 37°C for 12 h. After that, the culture was centrifuged at 4000 rpm for 5 min to pellet cells. The cells were rinsed with PBS three times to remove residual macromolecules and other growth medium components. The concentration of bacteria was measured by the absorbance at 600 nm (OD_{600}) via a UV-vis spectrophotometer (UV-1800, Shimadzu, Japan).

2.4 Bacterial colony counting assay

AuAg/GDY@PEG (40 μg mL^{-1}) was mixed with bacterial suspension (1×10^7 CFU mL^{-1}) in 2 mL sterile water in a sterile culture tube, the mixture of bacteria and AuAg/GDY@PEG were irradiated under NIR (808 nm, 0.9 W cm^{-2}) for 10 min and stirred 2 h at 37 ºC. Then, diluents of bacterial suspensions (1, 10^{-2}, 10^{-4}, 10^{-6}) were prepared and 100 μL of each diluent was applied to LB agar. Incubated at 37°C for 24h to form colonies, and then count colonies. The bacteria treated with AuAg/GDY@PEG, NIR irradiation, and ultrapure water were prepared as control groups.

Minimum inhibitory concentration (IC_{50}) determination, investigation of AuAg/GDY@PEG bacteria interaction via electron microscope imaging, and hemolysis assay are shown in Supporting Information.

2.5 Preparation of the immune-AuAg/GDY@PEG complexes.

0.5 mL of 100 μg·mL^{-1} anti-*S. typhimurium* antibodies was mixed with 1 mL of 1mg·mL^{-1} AuAg/GDY@PEG solution. Reaction was carried out at room temperature on a shaker for 2 h, then 3 mL 2% bovine serum albumin (w/v) was added to the mixture. Then the mixture was incubated on a shaker for 2 h at room temperature to block the residual surface of the AuAg/GDY@PEG, and store at 4 ºC.

2.6 Immunoreaction protocol and photothermal measurement

Anti-*S. typhimurium* antibodies-coated 96-well microtiter plate were prepared by adding 100 μL of anti-*S. typhimurium* antibodies (10 μg mL^{-1}) in 50 mM sodium carbonate buffer (pH=9.6) to a polystyrene 96-well microtiter plate and coated overnight at 4 ºC. Then rinsed with 10 mM PBS (containing 0.05% Tween 20, pH 7.4) to remove unbounded antibodies. Then 10 mM PBS (containing 1.0wt % BSA, pH 7.4) were added and reacted at 37℃ for 60 min. Then rinsed with 10 mM PBS (containing 0.05% Tween 20, pH 7.4). 50 μL of different concentrations of *S. typhimurium* or *E. coli* or *S. aureus* standard to the microporous plate and shaked at room temperature for 30 min. After washing with PBS, 100 μL of AuAg/GDY@PEG (2 mg mL^{-1}) was added into the plate and incubated for 30 min. Then washed with 10 mM PBS, 100μL of PBS (10 mM, pH 7.4) was added to each well and irradiated for 10 min under NIR (808 nm, 0.9W cm^{-2}), after irradiation, the temperature of the solution was measured with an electronic thermometer.

3. Results and discussion

3.1 synthesis and characterization of AuAg/GDY@PEG

<Fig.1>

It was used Ag nanocubes as template which was reported by Xia's [39], after Ag nanocubes reacted with a certain amount of $HAuCl_4$ solution, AuAg with hollow interiors and porous walls were produced. The asprepared Ag nanocubes have uniform sizes of 59±5 nm (Fig. S1). Fig. 1a and Fig.S2 clearly showed that high-quality hollow porous AuAg with thin wall were successfully prepared, the high contrast between the core and the shell implies a hollow structure. The AuAg nanocages have uniform sizes of 65±5 nm. HRTEM images of AuAg (Fig. 1b) reveal crystal planes with lattice spacing of 0.210 nm, which correspond well to the characteristic (200) planes of Au. As shown in the Fig. 1c, AuAg is uniformly loaded on GDY, which proves the successful preparation of AuAg/GDY@PEG. The STEM elemental mapping (Fig. 1d

and Fig. S3) shows four elements involving Au, Ag, C, and N in N-GDQDs/AuAg NCs. The more crystalline and phase information could be identified by powder X-ray diffraction (XRD) patterns. Fig. 1e included the XRD patterns of pure Ag nanocubes, AuAg. Due to the similar lattice constants between Au and Ag, Ag nanocubes, AuAg and AuAg/GDY@PEG have almost the same pattern. The diffraction peaks of AuAg/GDY@PEG are (111), (200), (220), (311) and (222), which are the same as those of AuAg and Ag nanocubes. The UV-vis spectra in Fig. 1f show the transformation of Ag nanocubes into AuAg was also accompanied by the red shift of the longitudinal SPR peak from blue to the NIR region. AuAg and AuAg/GDY@PEG show the strong absorption in the range of 300-1200 nm and the SPR peaks around 808 nm. The chemical structure of AuAg/GDY@PEG was analyzed by Raman spectroscopy. As shown in Fig. 1g, two prominent peaks at 1395 and 1593 cm^{-1} stand for the D and G bands of GDY, two weak peaks at 1945 and 2155 cm^{-1} were attributed to the vibration of conjugated diyne. The surface composition and elemental state of AuAg/GDY@PEG were studied by X-ray photoelectron spectroscopy (XPS) (Fig. 1h). The two peaks of 83.2 and 86.8 eV were correspond to the Au 4f7/2 and 4f5/2 spin-orbit peaks and the doublets of 367.3 and 373.3 eV were index to Ag 3d5/2 and 3d3/2 spin–orbit peaks (Fig. 1g and k), respectively. The characteristic peaks of C=C (283.9 eV), C≡C (285.2 eV), C-O (287.4 eV), and C=O (288.2 eV) in the high-resolution C 1s spectra of GDY (Fig. 1i).

<Fig.2>

3.2 Photothermal property of AuAg/GDY@PEG

The photothermal property of this therapeutic system was checked under the irradiation of an 808 nm NIR (0.9 W cm^{-2}, 10 min). As shown in Fig. 2a and b, the temperature of AuAg/GDY@PEG gradually rose with the irradiation time, whereas the

temperature of water hardly increased under the same condition. The temperatures of the AuAg/GDY@PEG, AuAg/GDY, AuAg+GDY, AuAg and GDY increase by 45.6, 43, 40, 38.6 and 17.8 ^{o}C under 808 nm NIR light irradiation after 10 min, this indicates that AuAg/GDY@PEG has good photothermal conversion ability, and enhanced photothermal effect is obtained through the combination of AuAg and GDY. The modification of PEG enhanced the biocompatibility of the material, and also improved the dispersion of the material, and further improved the photothermal conversion ability of the AuAg/GDY. The temperature change of AuAg/GDY@PEG can be better visualized by real-time thermal imaging photos in Fig. 2f. The nanomaterials we prepared can be heated up rapidly to more than 60 ^{o}C during NIR irradiation, which was enough to kill bacterial. Besides, the photothermal conversion capability was dependent on NIR irradiation power and sample concentration. The temperature of the AuAg/GDY@PEG solution increased with the enhanced NIR irradiation power (Fig. S4). After 10 min, the temperatures of the AuAg/GDY@PEG increase by 6.7, 13.6, 20.5, 30.6, and 45.6 ^{o}C with the powers of 0.3, 0.4, 0.5, 0.7, and 0.9 W cm^{-2}, respectively. As the concentration increased from 10 to 100 μg mL^{-1}(Fig. 2c), the temperatures of the above samples were increase by 16.1, 22, 34.6, 45.6, and 49.4 ^{o}C, respectively. In order to measure the performance of photothermal property quantitatively, the photothermal conversion efficiency of the AuAg/GDY@PEG solution was calculated, and the value was 47.7%, which is higher than the AuAg (η = 36.9%) and GDY (η = 22.5%) (Fig. 2d and S5). The photostability of AuAg/GDY@PEG was further investigated by performing six cycles of laser on/off with NIR irradiation (808 nm, 0.9 W cm^{-2}) (Fig. 2e). Compared to the temperature change after the first NIR irradiation, negligible fluctuation of the temperature elevation of sample solution was observed for next four additional cycles which shows that it has good stability and excellent

photothermal conversion ability. The high NIR absorbance and strong photothermal performances of AuAg/GDY@PEG make them superior as an encouraging photothermal agent.

<Fig.3>

3.3 Elimination of bacterial by photothermal effect of AuAg/GDY@PEG

The antibacterial activity of AuAg/GDY@PEG against Gram-positive *S. aureus* and Gram-negative *E. coli* was investigated under conditions with or without 808 nm NIR irradiation. The antibacterial effect of GDY alone on bacterial activity is greater than that of AuAg (Fig. S6 and S7). When bacteria come into contact with GDY, physical adsorption may lead to wrapping of bacterial membranes. The sharp edges of GDY nanosheets can insert into the bacterial membranes and cause the leakage of intracellular matrix. Concurrently, GDY can induce ROS chemically that interferes with specific microbial processes [36]. The activity of AuAg is associated with the release of Ag+ and the interaction between the high-energy surface of AuAg and the bacterial surface [44, 45]. In the absence of NIR light, the antibacterial action of GDY plays a major role. The decrease degree of bacterial activity in the GDY+NIR system is less than that in AuAg+NIR system under infrared irradiation. Since the temperature rise of GDY under NIR irradiation is limited, the increase of its antibacterial activity is low. The combination of AuAg+NIR can produce a large amount of heat to eradicate bacteria. Thus, the heat generated by AuAg under NIR irradiation has a dominant impact. AuAg/GDY@PEG treatment without laser irradiation caused obvious reduction in bacterial viability, while bacteria treated with NIR alone showed almost unchanged in bacterial viability (Fig. 3a, b, c and d). We attributed this to the antibacterial activity of AuAg/GDY@PEG may be contributed to a synergistic mechanism of wrapping, insertion, disruption, and oxidative stress on bacterial membrane by GDY, Remarkably,

808 nm NIR irradiation further strengthened th interaction between the high-energy surface of AuAg and the bacterial surface and release of Ag^+. e bactericidal effect of AuAg/GDY@PEG, no bacteria could be even found when AuAg/GDY@PEG concentration was higher than 40 μg mL^{-1}. AuAg/GDY@PEG exhibits an approximate effect on *S. aureus* and *E. coli* AuAg/GDY@PEG against *S. aureus* and *E. coli* bacterial killing rate > 99.999%. Under NIR, AuAg/GDY@PEG can be quickly released a large amount of heat, which was enough to further kill bacteria. Additionally, the half-maximum inhibitory concentrations (IC_{50}) of the AuAg/GDY@PEG determined as 32.68 μg mL^{-1} and 27.08 μg mL^{-1} for *S. aureus* and *E. coli* (Fig. S8). To explore the morphological change of bacteria, SEM analysis was performed after different treatments (Fig. 3e and f). It was clearly observed that a large portion of *S. aureus* and *E. coli* were bound to the nanosheets and the nanosheet was combined with the hollow nanocage, indicating the strong interactions between bacteria and nanosheets. AuAg/GDY@PEG was attached to the surface of the bacteria, and the bacteria had obvious deformation and the cell membrane became rough, indicating that AuAg/GDY@PEG+NIR caused bacterial damage. The biocompatibility was evaluated by hemolysis test and MTT assay (Fig. S9 and S10), compared with the 2% Triton X-100 positive group, there was no obvious hemolysis phenomenon even when the material concentration reached 100 μg mL^{-1}. After treatment with AuAg/GDY@PEG at a concentration of 100 μg ml^{-1} for 24 or 48h, the cell viability remained above 85%, showing no obvious cytotoxicity, indicating that AuAg/GDY@PEG had good biocompatibility.

<Fig.4>

3.4 AuAg/GDY@PEG-based photothermal immunoassay for *S. typhimurium* detection

S. typhimurium is one of the major pathogens that cause acute gastroenteritis and food poisoning [46]. Therefore, it is very important to detect trace *S. typhimurium*. AuAg/GDY@PEG-based photothermal immunoassay was employed for the determination of *S. typhimurium* standards with different concentrations on the anti-*S. typhimurium* antibodies-coated microplates with a sandwich structure. The temperatures were recorded on a digital thermometer after 10 min NIR irradiation (808 nm, 0.9W cm^{-2}). The procedure of *S. typhimurium* detection was shown in the Fig. 4a. In the case of the presence of only anti-*S. typhimurium* antibodies or anti-*S. typhimurium* plus *S. typhimurium*, no significant temperature change under the irradiation of NIR. After the addition of AuAg/GDY@PEG, an obvious temperature change was observed. The effect of immunoreaction time was optimized to obtain the best detection signal, the results was shown in Fig. 4b, when the immunoreaction time was less than 30 min, a rapidly temperature rise with the increase of immunoreaction time, the temperature changes can be ignored after 30 min, thus, 30 min was selected as the optimum immunoreaction time. Fig. 4c displays the temperature responses of AuAg/GDY@PEG-based photothermal immunoassay toward target *S. typhimurium* standards with various concentrations. The temperature variations were not obvious at low concentrations (1×10^{1}-1×10^{2} CFU·mL^{-1}) and high concentrations (1×10^{7}-1×10^{8} CFU·mL^{-1}), a good linear relationship between ΔT and the decimal logarithm of *S. typhimurium* concentrations were achieved within the range from 1×10^{3} to 1×10^{7} CFU·mL^{-1}. The LOD was defined as 3 times the noise level, obtained with 10 blank ΔT measured under optimal experimental conditions. The standard deviation of the mean blank ΔT was 0.28 °C and was considered as the value of the noise. Therefore, the LOD

was calculated to be 10^3 CFU·mL^{-1}. The regression equation was ΔT (°C) = -6.8 + 2.9 × log (CFU mL^{-1}). We compared our method with photothermal immunoassay methods and other methods, our method shows a great reliability, and has the advantages of high detection sensitivity and wide detection range (Table. 1).

S. aureus and *E. coli* were chosen as non-target bacteria to evaluate the specificity of this method. As shown in Fig. 4d, the ΔT of *S. typhimurium* was higher than with *S. aureus* and *E. coli*, these results indicate that AuAg/GDY@PEG-based photothermal immunoassay has satisfactory specificity. Tap water, juice and milk were selected to evaluate the accuracy of the photothermal immunoassay developed (Fig. 4e), with no *S. typhimurium* after sterilizing at 120 °C for 20 min. Different known amounts of *S. typhimurium* (10^3, 10^4, 10^5, 10^6 CFU·mL^{-1}) within the linear range of the AuAg/GDY@PEG-based photothermal immunoassay were spiked into the real samples and prepared as described above. The data in Fig. 4e showed that the recovery ranged from 96.4±4.4% (n = 3) to 105± 4.5% (n = 3) in tap water, 90.4 ± 3.5% (n = 3) to 109.2 ± 4.2% (n = 3) in milk and 97.8 ±3.2% (n = 3) to 107.2 ± 4.9% (n = 3) in juice. These results indicated that the proposed AuAg/GDY@PEG-based photothermal immunoassay hold a promising for the detection of *S. typhimurium* in real samples.

4. **Conclusions**

In summary, we have developed AuAg/GDY@PEG as an effective photothermal agent based on its excellent photothermal conversion capability. AuAg/GDY@PEG-based photothermal immunoassay was employed for determination of *S. typhimurium*. Moreover, AuAg/GDY@PEG demonstrated impressive broad-spectrum antibacterial properties due to the NIR-mediated hyperthermia, against *S. aureus* and *E. coli* with the killing rate >99.999%. In comparison with conventional approaches, the proposed photothermal immunoassay method displays advantages involving speediness,

simplicity, and low cost. This rapid detection method has the potential for applications in the on-site detection of pathogenic bacteria in food.

Declaration of Competing Interest

The authors declare no conflicts of interest.

Acknowledgements

This work was supported by the National Natural Science Foundation of China (Grant No. 21501106, 31800800), Natural Science Foundation of Shandong Province (Grant No. ZR2019BC101, ZR2020MB026, ZR202103010467), and Qingdao Municipal Science and Technology Commission (Grant No. 19-6-2-73-cg, 16-5-1-86-jch).

Reference:

[1] Q. Li, Y. Zhang, X. Huang, D. Yang, L. Weng, C. Ou, X. Song, X. Dong, An NIR-II light responsive antibacterial gelation for repetitious photothermal/thermodynamic synergistic therapy, Chem. Eng. J. 407 (2021) 127200.

[2] M. Jia, J. Liu, J. Zhang, H. Zhang, An immunofiltration strip method based on the photothermal effect of gold nanoparticles for the detection of Escherichia coli O157:H7, Analyst 144(2) (2019) 573-578.

[3] L. Wang, S. Li, J. Yin, J. Yang, Q. Li, W. Zheng, S. Liu, X. Jiang, The Density of Surface Coating Can Contribute to Different Antibacterial Activities of Gold Nanoparticles, Nano Lett. 20(7) (2020) 5036-5042.

[4] X. Gu, Z. Xu, L. Gu, H. Xu, F. Han, B. Chen, X. Pan, Preparation and antibacterial properties of gold nanoparticles: a review, Environ. Chem. Lett. 19(1) (2021) 167-187.

[5] W. Ma, X. Chen, L. Fu, J. Zhu, M. Fan, J. Chen, C. Yang, G. Yang, L. Wu, G. Mao, X. Yang, X. Mou, Z. Gu, X. Cai, Ultra-efficient Antibacterial System Based on Photodynamic Therapy and CO Gas Therapy for Synergistic Antibacterial and Ablation Biofilms, ACS Appl. Mater. Interfaces 12(20) (2020) 22479-22491.

[6] S. Liu, L. Wei, L. Hao, N. Fang, M.W. Chang, R. Xu, Y. Yang, Y. Chen, Sharper and Faster "Nano Darts" Kill More Bacteria: A Study of Antibacterial Activity of Individually Dispersed Pristine Single-Walled Carbon Nanotube, ACS Nano 3(12) (2009) 3891-3902.

[7] O. Akhavan, E. Ghaderi, Toxicity of Graphene and Graphene Oxide Nanowalls Against Bacteria, ACS Nano 4(10) (2010) 5731-5736.

[8] J. Shi, F. Zhang, S. Wu, Z. Guo, X. Huang, X. Hu, M. Holmes, X. Zou, Noise-free microbial colony counting method based on hyperspectral features of agar plates, Food Chem. 274 (2019) 925-932.

[9] W.H. Chin, Y. Sun, J. Høgberg, T.L. Quyen, P. Engelsmann, A. Wolff, D.D. Bang, Direct PCR – A rapid method for multiplexed detection of different serotypes of Salmonella in enriched pork meat samples, Mol. Cell. Probe. 32 (2017) 24-32.

[10] S. Niyomdecha, W. Limbut, A. Numnuam, P. Kanatharana, R. Charlermroj, N.

Karoonuthaisiri, P. Thavarungkul, Phage-based capacitive biosensor for Salmonella detection, Talanta 188 (2018) 658-664.

[11] S. Wu, A. Li, X. Zhao, C. Zhang, B. Yu, N. Zhao, F.-J. Xu, Silica-Coated Gold–Silver Nanocages as Photothermal Antibacterial Agents for Combined Anti-Infective Therapy, ACS Appl. Mater. Interfaces 11(19) (2019) 17177-17183.

[12] W. Jiang, Z. Zhang, Q. Wang, J. Dou, Y. Zhao, Y. Ma, H. Liu, H. Xu, Y. Wang, Tumor Reoxygenation and Blood Perfusion Enhanced Photodynamic Therapy using Ultrathin Graphdiyne Oxide Nanosheets, Nano Lett. 19(6) (2019) 4060-4067.

[13] D. Wang, M. Tang, H. Jiang, M. Li, S. Jiang, L. Sun, J. Sun, Helical bowl-like SnS2 with structure-induced conversion efficiency for enhanced photothermal therapy, Chem. Eng. J. 400 (2020) 125814.

[14] M. Xu, Y. Hu, Y. Xiao, Y. Zhang, K. Sun, T. Wu, N. Lv, W. Wang, W. Ding, F. Li, B. Qiu, J. Li, Near-Infrared-Controlled Nanoplatform Exploiting Photothermal Promotion of Peroxidase-like and OXD-like Activities for Potent Antibacterial and Anti-biofilm Therapies, ACS Appl. Mater. Interfaces 12(45) (2020) 50260-50274.

[15] C. Cao, W. Ge, J. Yin, D. Yang, W. Wang, X. Song, Y. Hu, J. Yin, X. Dong, Mesoporous Silica Supported Silver–Bismuth Nanoparticles as Photothermal Agents for Skin Infection Synergistic Antibacterial Therapy, Small 16(24) (2020) 2000436.

[16] L. Kong, F. Yuan, P. Huang, L. Yan, Z. Cai, T. Lawson, W. Wu, S. Chou, Y. Liu, A Metal–Polymer Hybrid Biomimetic System for use in the Chemodynamic-Enhanced Photothermal Therapy of Cancers, Small 16(43) (2020) 2004161.

[17] L. Li, H. Liu, J. Bian, X. Zhang, Y. Fu, Z. Li, S. Wei, Z. Xu, X. Liu, Z. Liu, D. Wang, D. Gao, Ag/Pd bimetal nanozyme with enhanced catalytic and photothermal effects for ROS/hyperthermia/chemotherapy triple-modality antitumor therapy, Chem. Eng. J. 397 (2020) 125438.

[18] J. Wang, Y. Chang, H. Luo, W. Jiang, L. Xu, T. Chen, X. Zhu, Designing immunogenic nanotherapeutics for photothermal-triggered immunotherapy involving reprogramming immunosuppression and activating systemic antitumor responses, Biomaterials 255 (2020) 120153.

[19] Y. Yang, D. Zhu, Y. Liu, B. Jiang, W. Jiang, X. Yan, K. Fan, Platinum-carbon-

integrated nanozymes for enhanced tumor photodynamic and photothermal therapy, Nanoscale 12(25) (2020) 13548-13557.

[20] Z. Zhang, J. Sun, X. Chen, G. Wu, Z. Jin, D. Guo, L. Liu, The synergistic effect of enhanced photocatalytic activity and photothermal effect of oxygen-deficient Ni/reduced graphene oxide nanocomposite for rapid disinfection under near-infrared irradiation, J. Hazard. Mater. 419 (2021) 126462.

[21] D. Xi, M. Xiao, J. Cao, L. Zhao, N. Xu, S. Long, J. Fan, K. Shao, W. Sun, X. Yan, X. Peng, NIR Light-Driving Barrier-Free Group Rotation in Nanoparticles with an 88.3% Photothermal Conversion Efficiency for Photothermal Therapy, Adv. Mater. 32(11) (2020) 1907855.

[22] X. Han, S. Lin, Y. Li, C. Cheng, X. Han, Near-infrared photothermal immunoassay for pancreatic cancer biomarker CA 19-9 on a digital thermometer, Anal. Chim. Acta 1098 (2020) 117-124.

[23] L. Lu, Y. Ge, X. Wang, Z. Lu, T. Wang, H. Zhang, S. Du, Rapid and sensitive multimode detection of Salmonella typhimurium based on the photothermal effect and peroxidase-like activity of MoS2@Au nanocomposite, Sensor. Actuat. B-Chem. 326 (2021) 128807.

[24] G. Li, Y. Li, H. Liu, Y. Guo, Y. Li, D. Zhu, Architecture of graphdiyne nanoscale films, Chem. Commun. 46(19) (2010) 3256-3258.

[25] X. Gao, H. Liu, D. Wang, J. Zhang, Graphdiyne: synthesis, properties, and applications, Chem. Soc. Rev. 48(3) (2019) 908-936.

[26] C. Huang, Y. Li, N. Wang, Y. Xue, Z. Zuo, H. Liu, Y. Li, Progress in Research into 2D Graphdiyne-Based Materials, Chem. Rev. 118(16) (2018) 7744-7803.

[27] Z. Zuo, Y. Li, Emerging Electrochemical Energy Applications of Graphdiyne, Joule 3(4) (2019) 899-903.

[28] Y. Du, W. Zhou, J. Gao, X. Pan, Y. Li, Fundament and Application of Graphdiyne in Electrochemical Energy, Accounts Chem. Res. 53(2) (2020) 459-469.

[29] X.-P. Yin, H.-J. Wang, S.-F. Tang, X.-L. Lu, M. Shu, R. Si, T.-B. Lu, Engineering the Coordination Environment of Single-Atom Platinum Anchored on Graphdiyne for Optimizing Electrocatalytic Hydrogen Evolution, Angew. Chem. Int. Edit. 57(30)

(2018) 9382-9386.

[30] S. Li, Y. Chen, H. Liu, Y. Wang, L. Liu, F. Lv, Y. Li, S. Wang, Graphdiyne Materials as Nanotransducer for in Vivo Photoacoustic Imaging and Photothermal Therapy of Tumor, Chem. Mater. 29(14) (2017) 6087-6094.

[31] Q. Bai, C. Zhang, L. Li, Z. Zhu, L. Wang, F. Jiang, M. Liu, Z. Wang, W.W. Yu, F. Du, Z. Yang, N. Sui, Subsequent monitoring of ferric ion and ascorbic acid using graphdiyne quantum dots-based optical sensors, Microchim. Acta 187(12) (2020) 657.

[32] C. Zhang, Y. Zhang, H. Xiao, J. Zhang, L. Li, L. Wang, Q. Bai, M. Liu, Z. Wang, N. Sui, Superior catalytic performance and CO tolerance of PtCu/graphdiyne electrocatalyst toward methanol oxidation reaction, Colloid. Surface. A. 612 (2021) 125960.

[33] Y. Fang, Y. Xue, L. Hui, H. Yu, Y. Li, Graphdiyne@Janus Magnetite for Photocatalytic Nitrogen Fixation, Angew. Chem. Int. Edit. 60(6) (2021) 3170-3174.

[34] J. Jin, M. Guo, J. Liu, J. Liu, H. Zhou, J. Li, L. Wang, H. Liu, Y. Li, Y. Zhao, C. Chen, Graphdiyne Nanosheet-Based Drug Delivery Platform for Photothermal/Chemotherapy Combination Treatment of Cancer, ACS Appl. Mater. Interfaces 10(10) (2018) 8436-8442.

[35] H. Min, Y. Qi, Y. Zhang, X. Han, K. Cheng, Y. Liu, H. Liu, J. Hu, G. Nie, Y. Li, A Graphdiyne Oxide-Based Iron Sponge with Photothermally Enhanced Tumor-Specific Fenton Chemistry, Adv. Mater. 32(31) (2020) 2000038.

[36] Z. Zhu, Q. Bai, S. Li, S. Li, M. Liu, F. Du, N. Sui, W.W. Yu, Antibacterial Activity of Graphdiyne and Graphdiyne Oxide, Small 16(34) (2020) 2001440.

[37] T. Wang, Q. Bai, Z. Zhu, H. Xiao, F. Jiang, F. Du, W.W. Yu, M. Liu, N. Sui, Graphdiyne-supported palladium-iron nanosheets: A dual-functional peroxidase mimetic nanozyme for glutathione detection and antibacterial application, Chem. Eng. J. 413 (2021) 127537.

[38] X. Bi, Q. Bai, L. Wang, F. Du, M. Liu, W.W. Yu, S. Li, J. Li, Z. Zhu, N. Sui, J. Zhang, Boron doped graphdiyne: A metal-free peroxidase mimetic nanozyme for antibacterial application, Nano Res. 2022, 15 (2), 1446-1454.

[39] S.E. Skrabalak, L. Au, X. Li, Y. Xia, Facile synthesis of Ag nanocubes and Au

nanocages, Nat. Protoc. 2(9) (2007) 2182-2190.

[40] C. Kim, E.C. Cho, J. Chen, K.H. Song, L. Au, C. Favazza, Q. Zhang, C.M. Cobley, F. Gao, Y. Xia, L.V. Wang, In Vivo Molecular Photoacoustic Tomography of Melanomas Targeted by Bioconjugated Gold Nanocages, ACS Nano 4(8) (2010) 4559-4564.

[41] H. Cheng, D. Huo, C. Zhu, S. Shen, W. Wang, H. Li, Z. Zhu, Y. Xia, Combination cancer treatment through photothermally controlled release of selenous acid from gold nanocages, Biomaterials 178 (2018) 517-526.

[42] H. Sun, J. Su, Q. Meng, Q. Yin, L. Chen, W. Gu, Z. Zhang, H. Yu, P. Zhang, S. Wang, Y. Li, Cancer Cell Membrane-Coated Gold Nanocages with Hyperthermia-Triggered Drug Release and Homotypic Target Inhibit Growth and Metastasis of Breast Cancer, Adv. Funct. Mater. 27(3) (2017) 1604300.

[43] S. Chernousova, M. Epple, Silver as Antibacterial Agent: Ion, Nanoparticle, and Metal, Angew. Chem. Int. Edit. 52(6) (2013) 1636-1653.

[44] A. D'Agostino, A. Taglietti, P. Grisoli, G. Dacarro, L. Cucca, M. Patrini, P. Pallavicini, Seed mediated growth of silver nanoplates on glass: exploiting the bimodal antibacterial effect by near IR photo-thermal action and Ag+ release, RSC Adv. 6(74) (2016) 70414-70423.

[45] P. Pallavicini, G. Dacarro, A. Taglietti, Self-Assembled Monolayers of Silver Nanoparticles: From Intrinsic to Switchable Inorganic Antibacterial Surfaces, Eur. J. of Inorg. Chem. 2018(45) (2018) 4846-4855.

[46] Y. Wang, S. Su, S. Du, Y. Gao, Z. Xu, H. Zhang, Rapid Detection for Salmonella typhimurium by Conventional Resistive Temperature Sensor Based on Photothermal Effect of Carboxylated Graphene Oxide, Food Anal. Method. 13(9) (2020) 1755-1763.

[47] S. Du, Y. Wang, Z. Liu, Z. Xu, H. Zhang, A portable immune-thermometer assay based on the photothermal effect of graphene oxides for the rapid detection of Salmonella typhimurium, Biosens. Bioelectron. 144 (2019) 111670.

[48] L. Zhao, J. Guo, S. Li, J. Wang, The development of thermal immunosensing for the detection of food-borne pathogens E. coli O157:H7 based on the novel substoichiometric photothermal conversion materials MoO3-x NPs, Sensor. Actuat. B-

Chem. 344 (2021) 130306.

[49] V. Shirshahi, S.N. Tabatabaei, S. Hatamie, R. Saber, Photothermal enhancement in sensitivity of lateral flow assays for detection of E-coli O157:H7, Colloid. Surface. B. 186 (2020) 110721.

[50] Z. Farka, T. Juřík, M. Pastucha, D. Kovář, K. Lacina, P. Skládal, Rapid Immunosensing of Salmonella Typhimurium Using Electrochemical Impedance Spectroscopy: the Effect of Sample Treatment, Electroanal. 28(8) (2016) 1803-1809.

[51] S. Ledlod, S. Areekit, S. Santiwatanakul, K. Chansiri, Colorimetric aptasensor for detecting Salmonella spp., Listeria monocytogenes, and Escherichia coli in meat samples, Food Sci. Technol. Int. 26(5) (2020) 430-443.

[52] S. Gao, L. He, Development of a filtration-based SERS mapping platform for specific screening of Salmonella enterica serovar Enteritidis, Anal. Bioanal. Chem. 411(29) (2019) 7899-7906.

[53] E. Makhneva, Z. Farka, P. Skládal, L. Zajíčková, Cyclopropylamine plasma polymer surfaces for label-free SPR and QCM immunosensing of Salmonella, Sensor. Actuat. B-Chem. 276 (2018) 447-455.

[54] L. Wang, R. Wang, F. Chen, T. Jiang, H. Wang, M. Slavik, H. Wei, Y. Li, QCM-based aptamer selection and detection of Salmonella typhimurium, Food Chem. 221 (2017) 776-782.

Scheme.1 Antibacterial study of AuAg/GDY@PEG and its detection of trace bacteria.

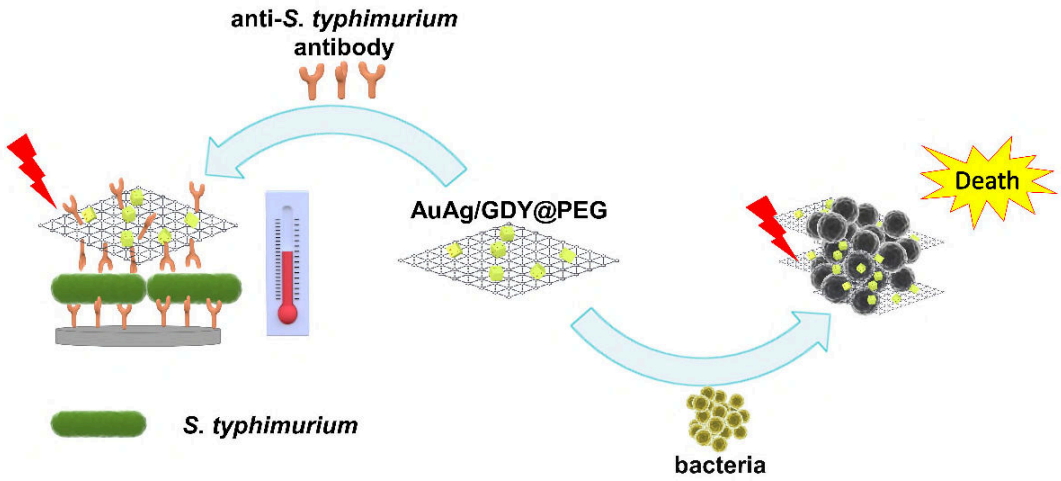

Fig. 1. (a, b) TEM and HRTEM images of AuAg. (c) TEM image of AuAg/GDY@PEG. (d) Scanning transmission electron microscopy (STEM) elemental mapping of AuAg/GDY@PEG. (e)XRD patterns of Ag nanocubes, AuAg and AuAg/GDY@PEG. (f) UV-vis spectra of Ag nanocubes, AuAg, GDY, AuAg/GDY@PEG. (g) Raman spectra of AuAg/GDY@PEG. High resolution XPS spectra of (h) AuAg/GDY@PEG. (i) C 1s, (j) Ag 3d, (k) Au 4f.

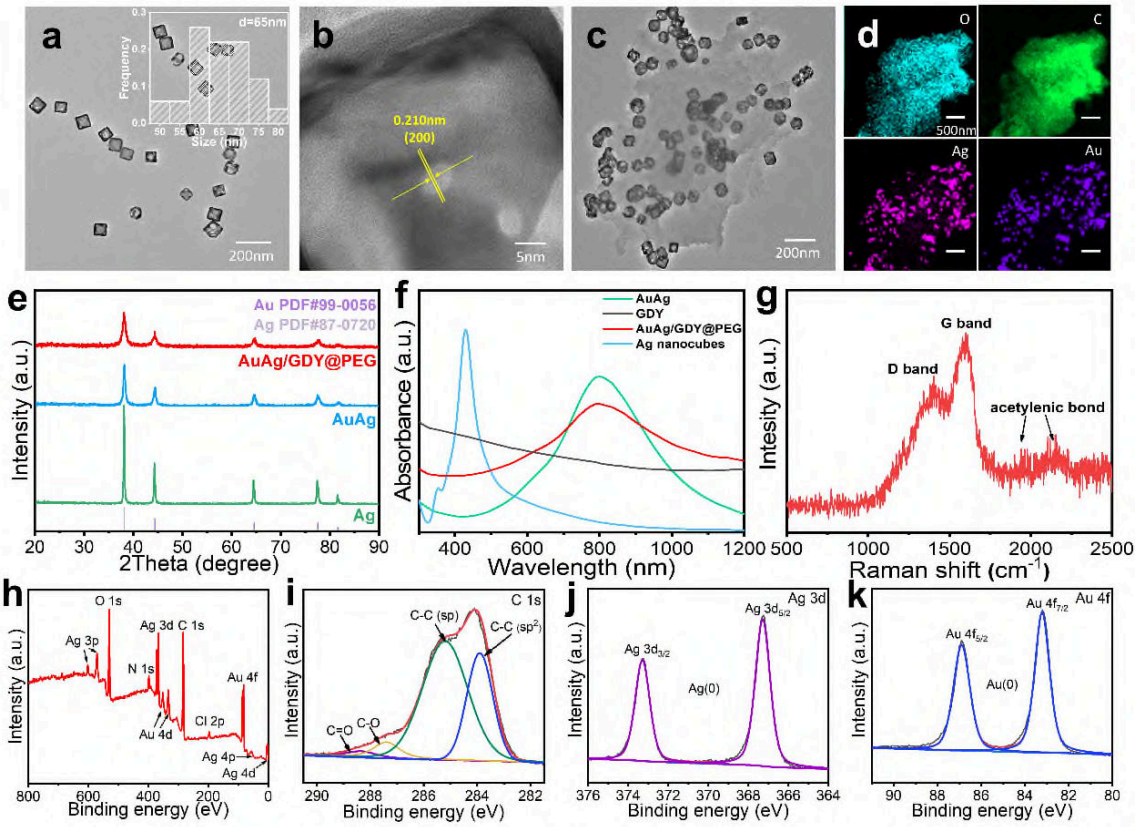

Fig. 2. (a, b) Comparison of photothermal conversion capabilities of different materials. (c)The corresponding temperature change curves of AuAg/GDY@PEG with gradient concentrations under NIR irradiation (808 nm, 0.9 W cm^{-2}, 10 min). (d) Calculation of photothermal conversion efficiency of AuAg/GDY@PEG. (e) The photothermal stability. (f) Infrared thermal images AuAg/GDY@PEG aqueous dispersions with different concentrations under 808 nm NIR irradiation.

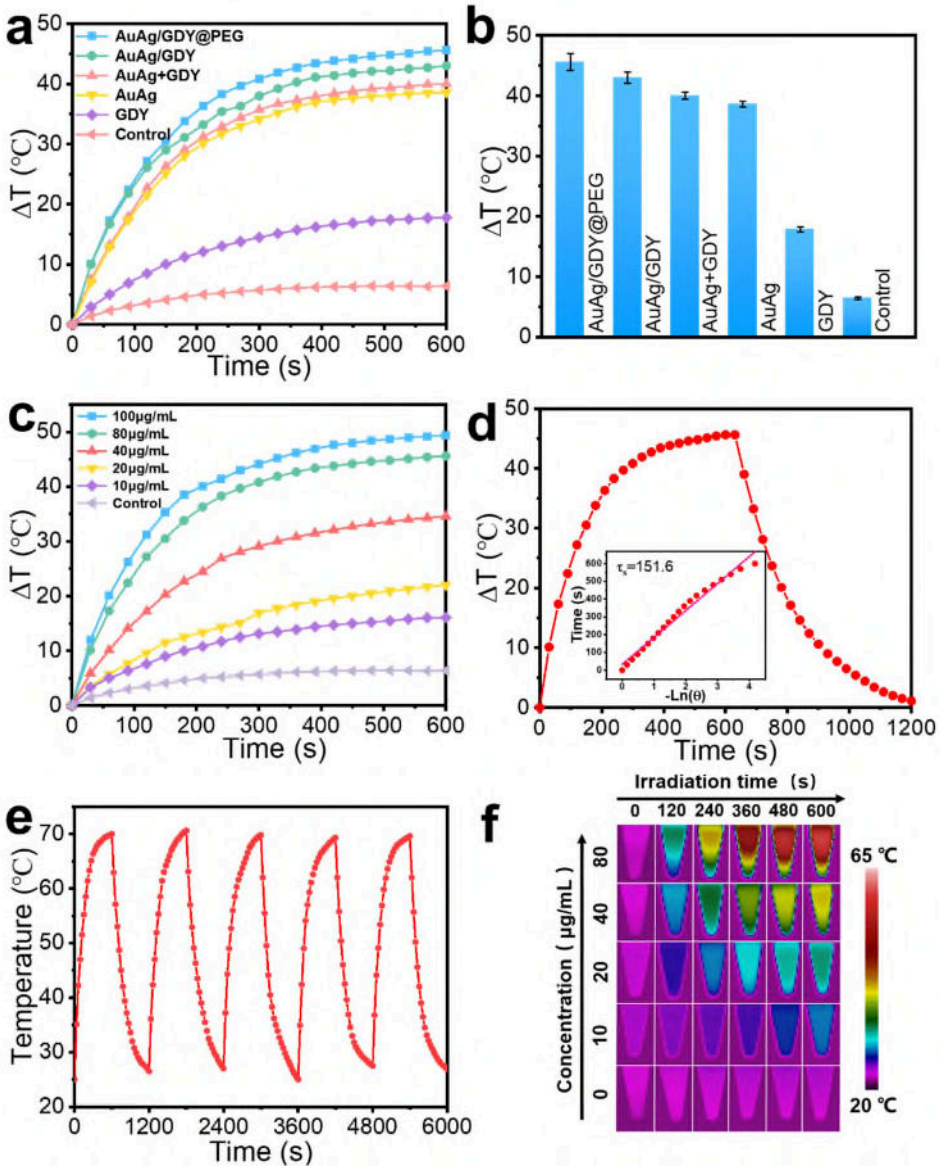

Fig. 3. (a,b) Photographs of the bacterial colonies formed by *S. aureus* and *E. coli* after different treatments. (c,d) Cell viability corresponding to (a,b). SEM images of the (e) *S. aureus* and (f) *E. coli* samples.

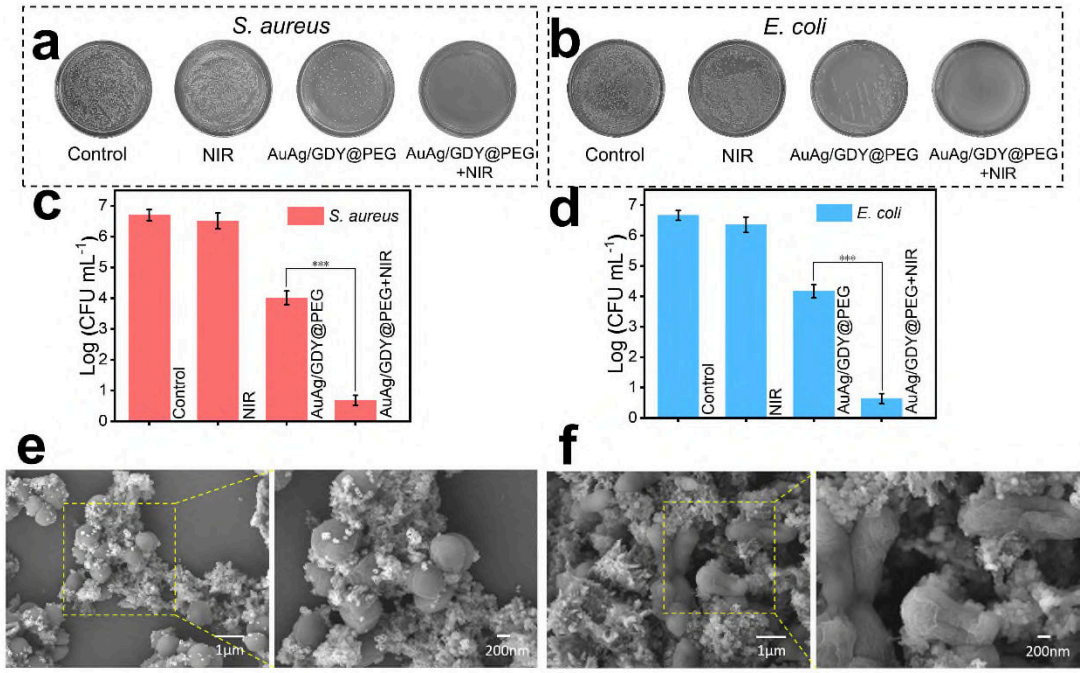

Fig. 4. (a) Procedure of *S. typhimurium* detection. (b) Effect of immunoreaction time on temperature. (c) Standard curve of the ΔT and the logarithm of the number of *S. typhimurium* concentration for the photothermal immunoassay. (d) Assessment of specificity. (e) Detection of *S. typhimurium* in water, milk and juice.

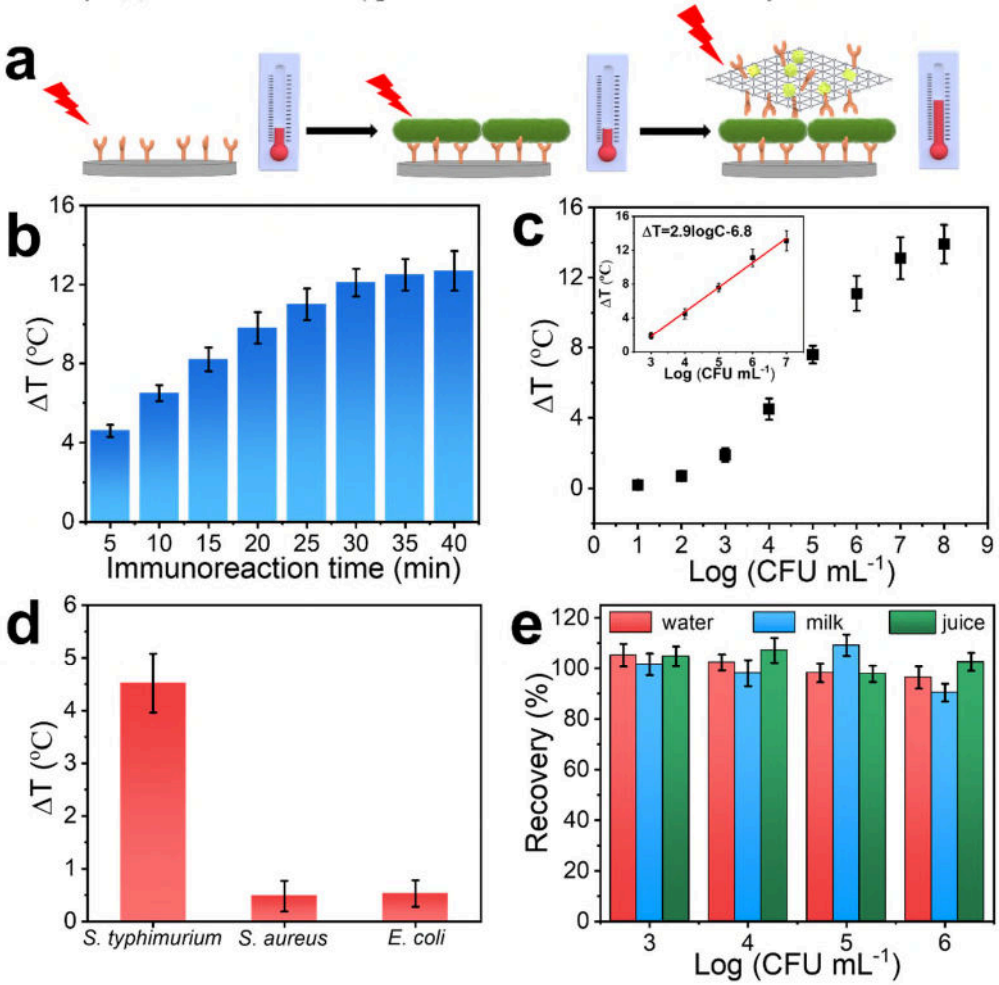

Table. 1. Comparation with other detection methods of pathogenic bacteria.

materials	Methods	Bacterial	Linear range (CFU mL^{-1})	LOD (CFU mL^{-1})	Ref
AuAg/GDY@PEG	Photothermal	S. Typhimurium	10^3-10^7	10^3	This work
GO	Photothermal	S. Typhimurium	10^3-10^9	10^3	[47]
GOs	Photothermal	S. Typhimurium	10^4-10^8	10^4	[46]
MoS_2@Au	Photothermal	S. Typhimurium	10^2-10^7	10^2	[23]
4-MBA MoO_{3-x} NPs	Photothermal	E. coli O157:H7	1.4×10^1-1.4×10^6	14	[48]
rGO	Photothermal	E. coli O157:H7	5×10^5-5×10^7	5×10^5	[49]
SPE	Electrochemical	S. Typhimurium	10^3-10^8	10^3	[50]
Ap6–AuNPs	Colorimetric	S. Enteritidis	10^5-10^8	10^5	[51]
Aptasensor	SERS	S. Enteritidis	1.4×10^3-1.4×10^7	1.4×10^3	[52]
CPA PP	SPR	S. Typhimurium	10^5-10^8	10^5	[53]
QCM-based aptasensor	Piezoelectric	S. Typhimurium	7.9×10^2-7.9×10^6	7.9×10^3	[54]

https://dspace.org/

AuAg nanocages/graphdiyne for rapid elimination and detection of trace pathogenic bacteria

Bai, Qiang; Luo, Hongyang; Shi, Shugao; Liu, Shen; Wang, Lina ...

2022-01-10
Elsevier
https://doi.org/10.1016/j.jcis.2022.01.046
Bai Q, Luo H, Shi S, et al., (2022) AuAg nanocages/graphdiyne for rapid elimination and detection of trace pathogenic bacteria. Journal of Colloid and Interface Science, Volume 613, May 2022, pp. 376-383

Downloaded from a DSpace repository. https://dspace.org/